Enhanced diffusion of boron by oxygen precipitation in heavily boron-doped silicon

Kazuhisa Torigoe[a] and Toshiaki Ono
Technology Division, Advanced Evaluation and Technology Development Department, SUMCO Corporation, 1-52 Kubara, Yamashiro-cho, Imari, Saga 849-4256, Japan

(Received 27 February 2017; accepted 16 May 2017; published online 1 June 2017)

The enhanced diffusion of boron has been investigated by analyzing out-diffusion profiles in the vicinity of the interface between a lightly boron-doped silicon epitaxial layer and a heavily boron-doped silicon substrate with a resistivity of 8.2 mΩ cm and an oxide precipitate (O.P.) density of 10^8–10^{10} cm^{-3}. It is found that the boron diffusion during annealing at 850–1000 °C is enhanced with the increase of the oxide precipitate density. On the basis of a model for boron diffusion mediated by silicon self-interstitials, we reveal that the enhanced diffusion is attributed to self-interstitials supersaturated as a result of the emission from oxide precipitates and the absorption by punched-out dislocations. In addition, the temperature dependence of the fraction of the self-interstitial emission obtained analyzing the diffusion enhancement well explains the morphology changes of oxide precipitates reported in literature. *Published by AIP Publishing.*
[http://dx.doi.org/10.1063/1.4984316]

I. INTRODUCTION

Diffusion of dopants in silicon such as boron, phosphorus, arsenic, and antimony has attracted great attention for allowing the accurate modeling of semiconductor device fabrication processing. Therefore, the mechanisms of dopant diffusion have been extensively investigated over the past decades.[1–10] It is well accepted that dopant diffusion in silicon can be mediated by native point defects, that is, silicon self-interstitials and vacancies whose concentrations are perturbed in the device fabrication processing such as oxidation, nitridation, and ion-implantation. For instance, phosphorus and antimony diffuse mediated by self-interstitials and vacancies, respectively.[7] On the other hand, arsenic diffuses via both point defect mechanisms.[7]

Boron, which is most widely used as a dopant in silicon devices, is known to diffuse mediated by self-interstitials. Boron diffusion is enhanced by the injection of self-interstitials due to oxidation of a silicon surface.[1–7] Packan and Plummer reported that the boron diffusivity during annealing in a dry O_2 ambient at 900–1100 °C increases by several to 10 times compared to annealing in an argon ambient.[4] On the other hand, boron diffusion is retarded by the injection of vacancies due to nitridation of a silicon surface,[11] suggesting that the supersaturated vacancies decrease the self-interstitial concentration due to the interstitial-vacancy recombination reaction. It is noted that the mechanisms of diffusion mediated by self-interstitials are divided into two different mechanisms, i.e., interstitialcy and kick-out mechanisms.[8,12–14] In the interstitialcy mechanism, boron diffuses via boron-interstitial pairs. In contrast, in the kick-out mechanism, boron on a substitutional site is kicked out by a silicon self-interstitial to an interstitial site and diffuses by hopping from one such site to another. Bracht *et al.* reported that boron diffuses mainly mediated by self-interstitials based on the comprehensive diffusion study using silicon isotope multilayer structures in the temperature range from 850 to 1100 °C.[9] Their analysis also reveals no significant contribution of boron-interstitial pairs to self-diffusion of silicon, suggesting either a small impact of boron-interstitial pairs on self-diffusion or that boron diffusion occurs via the kick-out mechanism rather than via the interstitialcy mechanism.[9]

Czochralski silicon (Cz-Si) crystals contain supersaturated oxygen atoms incorporated during crystal growth. It is well known that oxide precipitates formed during subsequent heat treatments are enhanced in heavily boron-doped Cz-Si,[15–21] resulting in oxide precipitates that act as strong gettering sinks to remove harmful metal impurities from the active region of devices. Therefore, the $p/p+$ silicon epitaxial wafer which consists of a lightly boron-doped epitaxial layer and a heavily boron-doped $p+$ substrate is used in high performance integrated circuit (IC) devices and high sensitive complementary metal oxide semiconductor (CMOS) image sensors. In general, it is also known that silicon self-interstitials are emitted from oxide precipitates to relax the compressive strain due to their volume expansion in a silicon matrix,[22–25] suggesting that the enhancement of boron diffusion due to the oxygen precipitation causes the change in resistivity of device regions in the epitaxial layer. On the other hand, oxide precipitates are accompanied with punched-out dislocations,[25,26] which act as sinks to absorb self-interstitials.[27] These self-interstitial emission and absorption effects on boron diffusion have not yet been reported.

In this paper, we investigate the dependence of boron diffusivity at 850–1000 °C on the density of oxide precipitates using $p/p+$ silicon epitaxial wafers. The obtained diffusivity is analyzed based on the model of boron diffusion mediated by silicon self-interstitials supersaturated as a

[a]Electronic mail: ktorigoe@sumcosi.com

result of the emission from oxide precipitates and the absorption by punched-out dislocations.

II. EXPERIMENTAL

p/*p*+ silicon epitaxial wafers were used in this study. *p*-type {100} silicon substrates with a thickness of about 700 μm were prepared from Cz-Si crystals heavily doped with boron. The boron concentration estimated from the electrical resistivity of the substrates (8.2 mΩ cm) obtained by four-point probe measurements was 1.1×10^{19} cm^{-3}, and the oxygen concentration was 12.9×10^{17} cm^{-3} using the old ASTM (1976) conversion factor. Silicon epitaxial layers with a thickness of about 2.5 μm were deposited on the substrates in a chemical vapor deposition (CVD) reactor at 1100–1150 °C for a few minutes using trichlorosilane as a gas source. The epitaxial layers were lightly doped with boron at the concentration of $\sim 10^{15}$ cm^{-3}. The depth profiles of boron concentration were obtained by secondary ion mass spectrometry (SIMS) using an O_2 primary ion beam having an energy of 8 keV.

In order to create the nuclei of oxide precipitates, the *p*/*p*+ silicon epitaxial wafers were annealed in a N_2 ambient in a horizontal furnace at 750 °C for 30 min, 700 °C for 5 min, and 700 °C for 4 h, respectively. It is confirmed by SIMS measurements performed after the heat treatments that the boron diffusion during annealing can be ignored. The wafers were cut into several pieces, which were used for the measurement of the density of oxide precipitates or the diffusion profile of boron after additional annealing.

To estimate the density of oxide precipitates, the wafers were introduced into a horizontal furnace at 900 °C and subsequently the temperature was raised at a rate of 5 °C/min up to 1000 °C followed by annealing for 16 h. The pits due to oxide precipitates were observed through an optical microscope at cleaved surfaces which had been etched about 2 μm in a Wright etchant.[28] The densities in bulk regions annealed at 750 °C for 30 min, 700 °C for 5 min, and 700 °C for 4 h were estimated to be 3×10^8 cm^{-3}, 3×10^9 cm^{-3}, and 3×10^{10} cm^{-3}, respectively.

For the boron diffusion, the epitaxial wafers with three different densities of oxide precipitates were annealed in a N_2 ambient in a horizontal furnace at 850 °C for 72 h, 900 °C for 48 h, 950 °C for 12–48 h, and 1000 °C for 8 h. Another wafer without oxide precipitates was annealed in a dry O_2 ambient in the horizontal furnace at 950 °C for 24 h as a reference. In the case of the annealing temperatures above 900 °C, the wafers were introduced into the furnace at 900 °C, and subsequently, the temperature was raised at a rate of 5 °C/min up to the annealing temperature to avoid the annihilation of the nuclei of oxide precipitates. The wafers annealed below 900 °C were introduced into the furnace at the annealing temperature. The thickness of the oxide layer formed when the samples were introduced from air to a N_2 ambient in the furnace was estimated to be about 4 nm by spectroscopic ellipsometry measurements, which prevents nitridation during annealing. After annealing, the depth profiles of boron concentration were obtained by SIMS measurements. Transmission electron microscopy (TEM) samples were prepared by mechanical polishing followed by argon ion milling. TEM observations for punched-out dislocations emitted by oxide precipitates were carried out along the [001] direction with acceleration voltages of 200 kV.

III. RESULTS AND DISCUSSION

A. Enhanced diffusivity of boron depending on the density of oxide precipitates

Figure 1 shows the depth profiles of boron concentration in *p*/*p*+ silicon epitaxial wafers with oxide precipitates of 3×10^8 cm^{-3}, 3×10^9 cm^{-3}, and 3×10^{10} cm^{-3} in density and without oxide precipitates after the epitaxial growth and after the different heat treatments at 850–1000 °C. The concentration in the epitaxial layer is here normalized to the bulk concentration. The short penetration of boron atoms from a substrate to an epitaxial layer is observed after the epitaxial growth at 1100–1150 °C for a few minutes. Out-diffusion of boron atoms from a substrate to an epitaxial layer mainly occurs during the heat treatments. It is clearly shown that the boron diffusion in wafers with oxide precipitates is enhanced compared to the diffusion in wafers without oxide precipitates, and the enhancement increases with increasing density of oxide precipitates. As one can see in Fig. 1(d), the enhancement of diffusion due to oxide precipitates is found to be smaller than oxidation enhanced diffusion observed in wafers after annealing at 950 °C for 24 h in a dry O_2 ambient.

We estimated the boron diffusivity enhanced by oxide precipitates by analyzing the SIMS out-diffusion profiles shown in Fig. 1. The profiles can be theoretically reproduced by numerically solving the one-dimensional diffusion equation based on Fick's law as follows:

$$\frac{\partial C}{\partial t} = \frac{\partial}{\partial x}\left(D\frac{\partial C}{\partial x}\right), \tag{1}$$

where C is the concentration of diffusing species as a function of time t and position x, and D is the diffusivity. The calculated depth profiles shown in Fig. 1 are in good agreement with the experimental results. Figure 2(a) shows the diffusivity of boron D_B as a function of the density of oxide precipitates. Each plot was obtained by the best fit to the out-diffusion profile in Fig. 1, and the obtained values of D_B are summarized in Table I. It is found that the diffusion enhancement ratio D_B/D_B^* increases with increasing density of oxide precipitates, where D_B^* is the boron diffusivity in wafers without oxide precipitates [Fig. 2(b)]. The magnitude of the enhancement due to oxide precipitates was less than a factor of 4.

B. An enhanced diffusion model by silicon self-interstitial supersaturated due to oxygen precipitation

It is well known that the boron diffusion in silicon is enhanced by the injection of silicon self-interstitials.[1–7] In general, the effective diffusivity of boron D_B is described by the sum of the contributions of diffusion mediated by self-interstitials and vacancies[1–7]

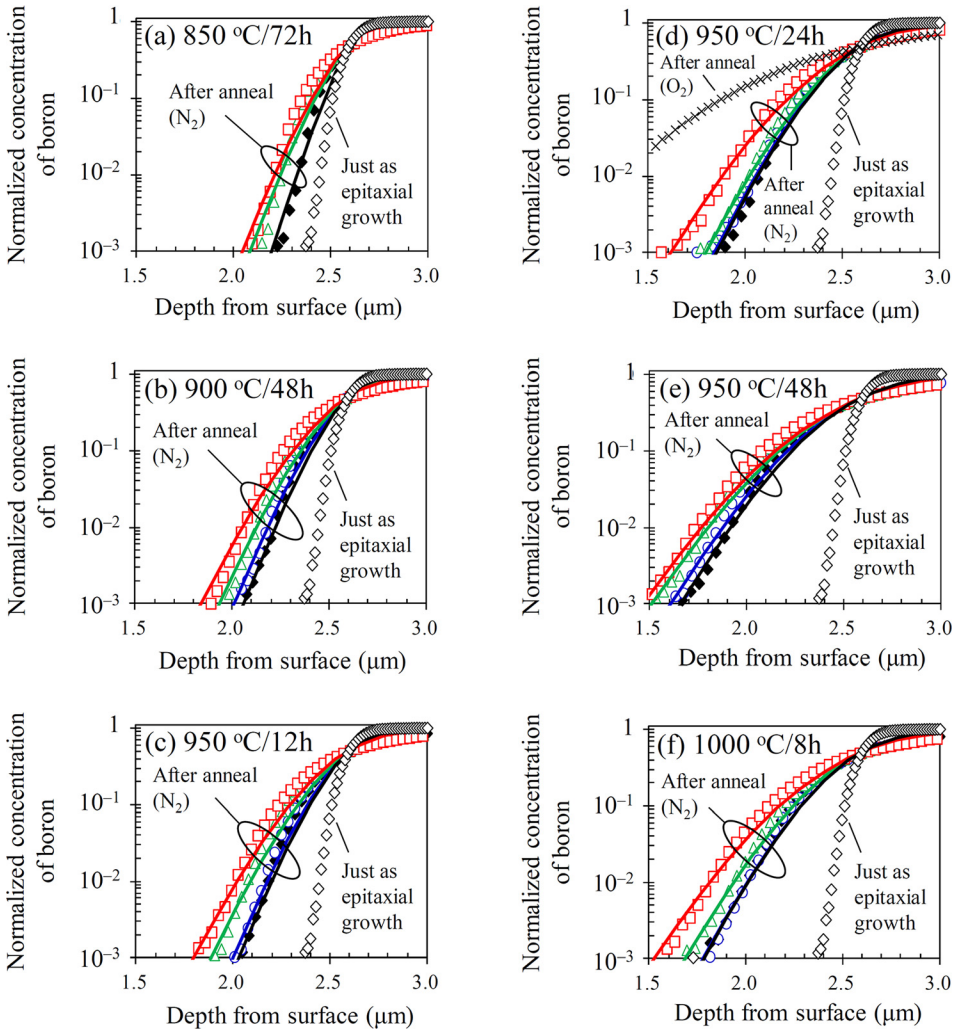

FIG. 1. Depth profiles of boron concentration in *p*/*p*+ epitaxial wafers just after epitaxial growth (open diamonds) and after annealing at 850 °C for 72 h in (a), 900 °C for 48 h in (b), 950 °C for 12 h in (c), 950 °C for 24 h in (d), 950 °C for 48 h in (e), and 1000 °C for 8 h in (f). Full diamonds show the profiles in wafers without oxide precipitates, and open circles, triangles, and squares show the profiles in wafers with oxide precipitates of $3\times10^{8}\,\mathrm{cm}^{-3}$, $3\times10^{9}\,\mathrm{cm}^{-3}$, and $3\times10^{10}\,\mathrm{cm}^{-3}$, respectively, after annealing in a N_2 ambient. The crosses in (d) show the profile after annealing in a dry O_2 ambient. The solid lines show best fits using Eq. (1).

$$\frac{D_B}{D_B^*}=f_{\mathrm{I}}\left(\frac{C_{\mathrm{I}}}{C_{\mathrm{I}}^{\mathrm{eq}}}\right)+(1-f_{\mathrm{I}})\left(\frac{C_{\mathrm{V}}}{C_{\mathrm{V}}^{\mathrm{eq}}}\right), \tag{2}$$

where f_{I} is the fraction of diffusion mediated by self-interstitials, C_{I} and C_{V} are the concentrations of self-interstitials and vacancies, respectively, $C_{\mathrm{I}}^{\mathrm{eq}}$ and $C_{\mathrm{V}}^{\mathrm{eq}}$ are the corresponding thermal equilibrium concentrations, and D_B^* is the diffusivity under the thermal equilibrium of self-interstitials and vacancies, i.e., $C_{\mathrm{I}}/C_{\mathrm{I}}^{\mathrm{eq}}=1$ and $C_{\mathrm{V}}/C_{\mathrm{V}}^{\mathrm{eq}}=1$. In the last two decades, several authors[4–7] have reported the values of f_{I} in the range of 0.80–0.99, suggesting that boron in silicon mainly diffuses via some mechanisms mediated by self-interstitials. Bracht *et al.*[9] reported that the analysis of the simultaneous diffusion of boron and silicon at temperatures between 850 °C and 1100 °C reveals no significant contribution of boron-interstitial pairs to self-diffusion, suggesting either a small fraction of self-diffusion *via* boron-interstitial pairs or that boron diffuses through the kick-out mechanism rather than by the interstitialcy mechanism.[9]

In order to analyze the boron diffusion enhancement in this study, it is reasonable to assume that the effective diffusivity of boron is determined by diffusion *via* self-interstitials ignoring the contribution of vacancies as described in the following relationship:

$$D_B=D_B^*\left(\frac{C_{\mathrm{I}}}{C_{\mathrm{I}}^{\mathrm{eq}}}\right). \tag{3}$$

The silicon self-interstitials are known to be emitted from oxide precipitates to relax the compressive strain due to their volume expansion, resulting in higher supersaturation of self-interstitials. Some of the self-interstitials are absorbed by the punched-out dislocations emitted by the oxide precipitates.[27] In this work, the flux of self-interstitials associated with oxygen precipitation is determined by the sum of the flux of self-interstitials emitted from an oxide precipitate J_{e} and the flux of self-interstitials absorbed by punched-out dislocations surrounding the oxide precipitate J_{a}

$$J=J_{\mathrm{e}}+J_{\mathrm{a}}. \tag{4}$$

The flux emitted from an oxide precipitate is given by

$$J_{\mathrm{e}}=\gamma_{\mathrm{I}}\times J_{\mathrm{O}}, \tag{5}$$

where γ_{I} is the fraction of self-interstitial emission and J_{O} is the flux of oxygen atoms consumed for the growth of an oxide precipitate. The shape of the platelet oxide precipitate is approximated as an oblate spheroidal.[22] The growth rate of the oxide precipitate, which corresponds to J_{O}, is limited by the diffusion of oxygen atoms[22]

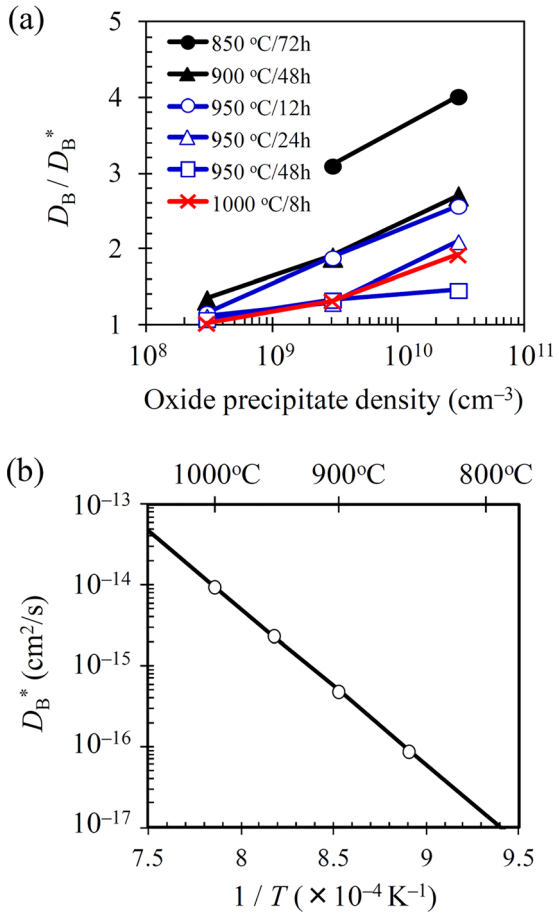

FIG. 2. (a) Dependence of the diffusion enhancement ratio of boron on the density of oxide precipitates. The values of diffusivities are summarized in Table I. (b) Temperature dependence of D_B^*.

$$J_O = 4\pi R D_O \frac{\beta}{\operatorname{arccot}(\beta/\sqrt{1-\beta^2})}\left(C_O - C_O^{int}\right), \quad (6)$$

where R and β are the radius and the aspect ratio of oxide precipitates, respectively, D_O is the diffusivity of oxygen in heavily boron-doped silicon,[29] C_O is the oxygen concentration, and C_O^{int} is the thermal equilibrium concentration of oxygen at the interface between an oxide precipitate and a silicon matrix, i.e., $C_O^{int} = C_O^{eq} \exp(\sigma\Omega_P/RkT)$, where C_O^{eq} is the thermal equilibrium concentration of oxygen in silicon crystals,[30] σ is the interfacial energy (688 erg/cm^2),[31] Ω_P is the specific volume of a SiO_2 molecule in a precipitate (4.42×10^{-23} cm^3),[25] k is the Boltzmann constant, and T is the temperature. It is noted that the value of R is defined as the radius of a spherical precipitate which has the same volume as a platelet precipitate. The absorption term for self-interstitials on the right-hand side in Eq. (4) is assumed to be limited by the diffusion of self-interstitials from an oxide precipitate to dislocations under the approximation that the dislocations are column shapes

$$J_a = -2\pi r L D_I (C_I^{int} - C_I^{eq})/\lambda, \quad (7)$$

where r is the radius of dislocations, L is the total length of dislocations emitted by an oxide precipitate, D_I is the diffusivity of self-interstitial,[32] C_I^{int} is the self-interstitial concentration at the interface between an oxide precipitate and a silicon matrix, and λ is the average distance between an oxide precipitate and dislocations. In Eq. (7), the self-interstitial concentration at the interface between a dislocation and a silicon matrix is considered to be the thermal equilibrium concentration in a silicon crystal C_I^{eq}.[32] The radius of a dislocation is taken to be $r = 0.5$ nm according to the previous studies for oxygen diffusion to a dislocation core.[33–35]

The relationship between λ and L was examined by TEM observations in order to estimate the absorption flux in Eq. (7). The typical bright-field TEM image of dislocations emitted from an oxide precipitate is shown in the inset of Fig. 3(a). Several punched-out dislocation loops near an oxide precipitate and one elongated dislocation loop are observed. The density of prismatic dislocation loops[26,27] are low in our samples. Almost all dislocations are complicated or elongated loops as shown in Fig. 3(a). The relationship between λ and L in the wafers with oxide precipitates of 3×10^{10} cm^{-3} in density is plotted in Fig. 3(a), which gives the empirical expression

$$\lambda = 1.4 \times 10^{-3} L^{0.47}\ (\text{cm}). \quad (8)$$

The dislocations should lie on a {111} plane. Therefore, the length L in Eq. (8) is obtained by projecting TEM images of a {100} plane on a {111} plane. Figure 3(b) shows the relationship between the measured values of L and the radius of an oxide precipitate R calculated using the flux of oxygen in Eq. (6) with the average aspect ratio β of 0.03 observed in $p/p+$ silicon epitaxial wafers,[21] which gives the following relationship:

$$L = 2.8 \times 10^{14} R^{3.4}\ (\text{cm}). \quad (9)$$

Accordingly, the absorption flux of self-interstitials by dislocations in Eq. (7) is described as a function of the radius of an oxide precipitate using Eqs. (8) and (9)

$$J_a \propto -R^{1.8} D_I (C_I^{int} - C_I^{eq}). \quad (10)$$

Taking into account the emission and absorption flux in Eqs. (5) and (10), respectively, the self-interstitial concentration as a function of the wafer depth x can be obtained by

$$\frac{dC_I(x)}{dt} = \nabla(D_I \nabla C_I(x)) + \int N(x,R)\{J_e(x,R) + J_a(x,R)\}dR, \quad (11)$$

TABLE I. Dependence of boron diffusivity (cm^2 s^{-1}) on the oxide precipitate density and the heat treatment temperature and time.

	Density of oxide precipitates (cm^{-3})			
Heat treatments	No[a]	3×10^{-8}	3×10^{-9}	3×10^{-10}
850 °C for 72 h	8.7×10^{-17}	…	2.7×10^{-16}	3.5×10^{-16}
900 °C for 48 h	4.8×10^{-16}	6.4×10^{-16}	9.1×10^{-16}	1.3×10^{-15}
950 °C for 12 h	2.3×10^{-15}	2.7×10^{-15}	4.4×10^{-15}	6.0×10^{-15}
950 °C for 24 h	2.5×10^{-15}	2.6×10^{-15}	3.0×10^{-15}	4.9×10^{-15}
950 °C for 48 h	2.2×10^{-15}	2.5×10^{-15}	3.1×10^{-15}	3.4×10^{-15}
1000 °C for 8 h	9.4×10^{-15}	9.5×10^{-15}	1.2×10^{-14}	1.8×10^{-14}

[a]No denotes that no precipitates were observed using the optical microscope.

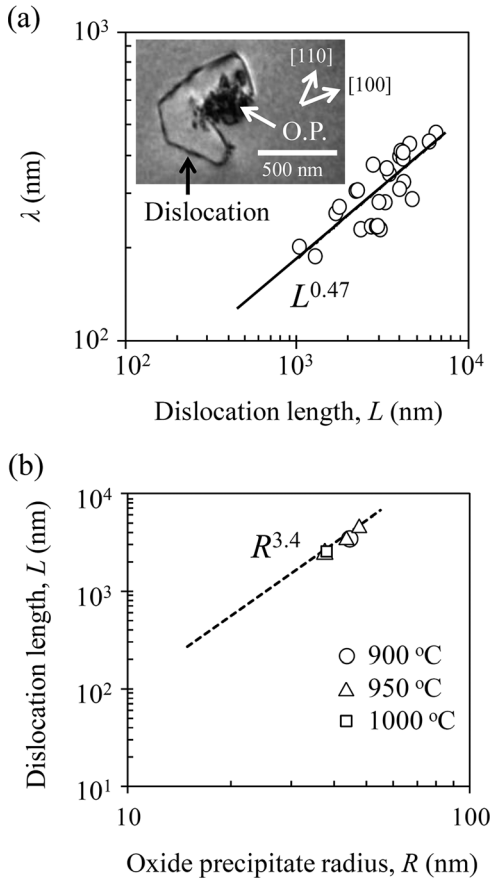

FIG. 3. (a) Average distance between an oxide precipitate and dislocations λ as a function of the dislocation length L. The inset indicates a typical bright-field TEM image of dislocations around an oxide precipitate (O.P.). (b) Dislocation length L as a function of the radius of oxide precipitate R after annealing at 900 °C (circles), 950 °C (triangles), and 1000 °C (squares).

where $N(x, R)$ is the density of oxide precipitates with radius R, which is assumed to be initially distributed only in the $p+$ substrate. The absorption flux is here described by

$$J_a(x,R) \propto -R^{1.8} D_I (C_I(x) - C_I^{eq}), \tag{12}$$

under the assumption that the self-interstitial concentration at the interface of an oxide precipitate C_I^{int} in Eq. (10) is replaced by the average concentration $C_I(x)$ in a silicon matrix of depth x because of the considerably large diffusivity of self-interstitials. The typical diffusion length $\sqrt{Dt}$ at 900 °C for 12 h is estimated to be ~1 cm using the diffusivity reported by Nakamura *et al.*,[32] which is considerably larger than the average distance between adjacent oxide precipitates of 15 μm for $3 \times 10^8\,cm^{-3}$ in density.

The radius R in the second term on the right-hand side of Eq. (11) depends on the oxygen concentration at depth x. The depth profile can be obtained by solving the diffusion equation in Eq. (1) using the oxygen diffusivity.[29] The boundary condition of oxygen and self-interstitial concentrations at the surface of the epitaxial wafer is considered to maintain the thermal equilibrium concentrations in silicon crystals as reported by Mikkelsen[36] and Nakamura *et al.*,[32] respectively. Finally, the change in the depth profile of boron concentration can be calculated by numerically solving the diffusion equation in Eq. (1) with the enhanced diffusivity of boron in Eq. (3) depending on the self-interstitial concentration supersaturated as a result of the emission from oxide precipitates and the absorption by punched-out dislocations. In this model the fraction of self-interstitial emission γ_I is a fitting parameter depending on temperature, which is discussed in Sec. III C.

C. Analysis of boron diffusion enhancement

Figure 4(a) shows the typical calculated depth profiles of the density and the radius of oxide precipitates, and the length of dislocations in the $p/p+$ epitaxial wafer after annealing at 950 °C for 12 h. In this calculation, the oxide precipitates of $3 \times 10^{10}\,cm^{-3}$ in density are assumed to be initially distributed in the $p+$ substrate and the fraction of self-interstitial emission γ_I is set to be 0.10. In the vicinity of the interface between the epitaxial layer and the $p+$ substrate, the out-diffusion of oxygen atoms to the wafer surface results in the smaller radius and length of oxide precipitates and dislocations, respectively. Figure 4(b) shows the calculated depth profiles of self-interstitial concentration and boron diffusivity. The total amount of self-interstitials emitted from oxide precipitates [see the solid line in Fig. 4(b)] can be obtained by the integration of the emission flux in Eq. (5) during annealing, which is estimated at $\sim 10^{16}\,cm^{-3}$ in the $p+$ substrate. Taking into account the out-diffusion of self-interstitials and the absorption by dislocations, the self-interstitial concentration reduces to $\sim 10^{10}\,cm^{-3}$ [see the dotted line in Fig. 4(b)]. The boron diffusivity increases in proportion to the supersaturation of the self-interstitial concentration (see the dashed line). It is noted that the

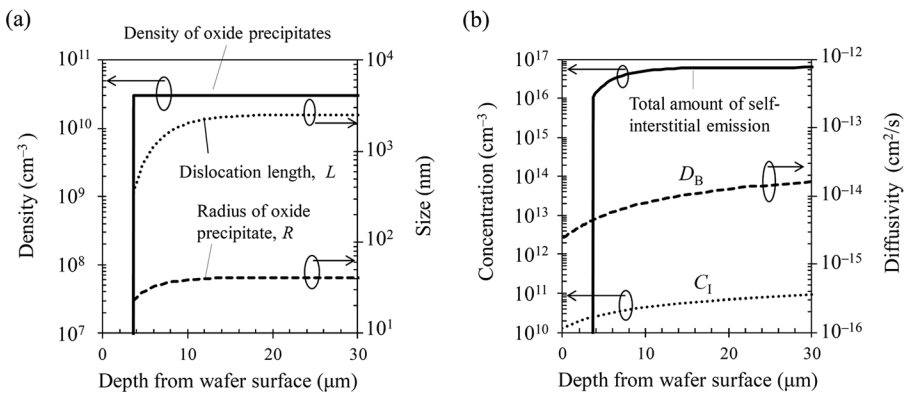

FIG. 4. Typical depth profiles of physical parameters after annealing for 12 h at 900 °C calculated by our model. (a) Density of oxide precipitates (solid line), radius of oxide precipitates (dashed line), and dislocation length (dotted line). (b) Total amount of silicon self-interstitial emission (solid line), diffusivity of boron D_B (dashed line), and concentration of self-interstitial C_I (dotted line). The fraction of self-interstitial emission γ_I is set to be 0.10.

self-interstitials maintain the thermal equilibrium concentration at the wafer surface, which yields $D_B = D_B^*$ at the surface. As one can see in Fig. 4(b), the boron diffusivity in the vicinity of the interface between the epitaxial layer and the $p+$ substrate is enhanced by a factor of ~2 relative to D_B^*.

Figure 5 shows the depth profiles of boron concentration in epitaxial wafers after annealing for 12 h at 950 °C. It is found that the out-diffusion profiles calculated considering both the emission of self-interstitials from oxide precipitates and the absorption by dislocations (see solid lines) well reproduce the experimental results in wafers with the oxide precipitates of $3 \times 10^8\,cm^{-3}$, $3 \times 10^9\,cm^{-3}$, and $3 \times 10^{10}\,cm^{-3}$ in density. On the other hand, the calculations ignoring the absorption effect strongly enhance the out-diffusion in the case of $3 \times 10^9\,cm^{-3}$ and $3 \times 10^{10}\,cm^{-3}$ in density.

Figure 6 shows the dependence of the diffusion enhancement ratio D_B/D_B^* on annealing time at 850, 900, 950, and 1000 °C. The calculated lines are here obtained using the diffusivity at the interface between an epitaxial layer and a $p+$ substrate. The calculated results well reproduce the experimental results. It is noted that the enhancement ratio in wafers with the oxide precipitate density of $3 \times 10^{10}\,cm^{-3}$ decreases during annealing because the emission flux of self-interstitials in Eq. (5) reduces due to the decrease of dissolved oxygen by its precipitation. The best fits to the experimental results give the fraction of self-interstitial emission γ_I of 0.014, 0.040, 0.10, and 0.23 for 850 °C, 900 °C, 950 °C, and 1000 °C, respectively. The obtained dependence of γ_I on temperature is shown in Fig. 7, which is found to decrease with decreasing temperature.

Sueoka *et al.* suggest that the fraction of self-interstitial emission is determined by the relationship between $D_O C_O^{eq}$ and $D_I C_I^{eq}$; the fraction is in proportion to $D_I C_I^{eq}/D_O C_O^{eq}$, which decreases with decreasing temperature.[22] The change in the fraction of the self-interstitial emission causes the morphology change of oxide precipitates depending on the temperature. The precipitate morphology is basically

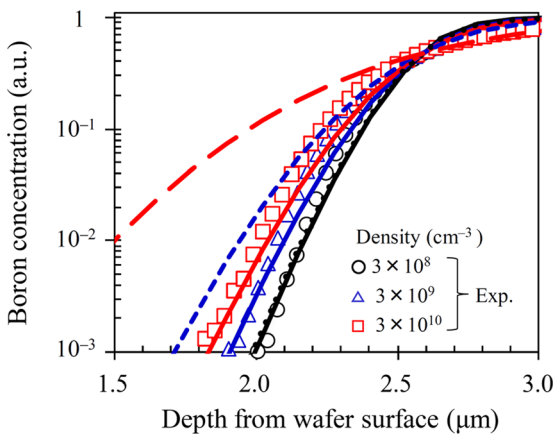

FIG. 5. Typical depth profiles of boron concentration after annealing at 950 °C for 12 h. The circles, triangles, squares show the experimental results obtained using $p/p+$ epitaxial wafers with oxide precipitates of $3 \times 10^8\,cm^{-3}$, $3 \times 10^9\,cm^{-3}$, and $3 \times 10^{10}\,cm^{-3}$, respectively. The solid lines are the corresponding calculated results obtained considering the absorption of self-interstitials by dislocations. The dotted, short-dashed, and long-dashed lines are the calculated results obtained ignoring the absorption in wafers with oxide precipitates of $3 \times 10^8\,cm^{-3}$, $3 \times 10^9\,cm^{-3}$, and $3 \times 10^{10}\,cm^{-3}$, respectively. The fraction of self-interstitial emission γ_I is set to be 0.10.

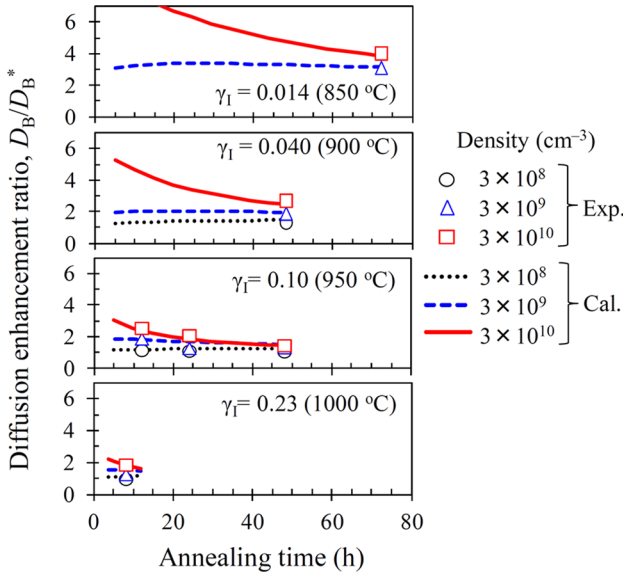

FIG. 6. Dependence of the diffusion enhancement ratio of boron on annealing time at 850 °C, 900 °C, 950 °C, and 1000 °C. The circles, triangles, and squares are the experimental results obtained using $p/p+$ epitaxial wafers with oxide precipitates of $3 \times 10^8\,cm^{-3}$, $3 \times 10^9\,cm^{-3}$, and $3 \times 10^{10}\,cm^{-3}$ in density, respectively. The dotted, dashed, and solid lines are the corresponding calculated results.

determined by the free energy associated with its strain energy and the interfacial energy.[37] At lower temperatures, the potential strain energy is very high due to the lower fraction of self-interstitial emission from oxide precipitates, resulting in the situation that platelet precipitates are favored to decrease the strain energy. Since at higher temperatures, the strain can be relaxed almost entirely due to the higher fraction of self-interstitial emission, the interfacial energy is dominant, which leads to a spherical geometry. The morphology of an oxide precipitate can be estimated using the values of γ_I obtained by the analysis of the enhanced diffusion of boron in this work under the assumption that the precipitate shape is determined by minimizing the excess free energy given by[22]

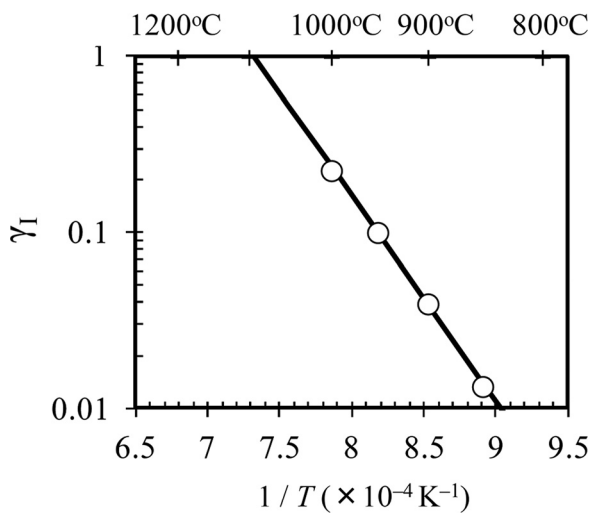

FIG. 7. Temperature dependence of the fraction of silicon self-interstitials emitted from an oxide precipitate.

$$G_E = G_\varepsilon + G_\sigma, \tag{13}$$

where G_ε and G_σ are the strain energy and the interfacial energy of a precipitate, respectively,

$$G_\varepsilon = \frac{4\pi R^3}{3} E(\beta) \frac{6\mu\delta^2}{1+4\mu/3K}, \tag{14}$$

$$G_\sigma = S(\beta, R)\sigma, \tag{15}$$

where $E(\beta)$ is the normalized strain energy of a precipitate as a function of β,[38] i.e., $E(1)=1$ for a sphere, μ and K are the shear modulus (7×10^{11} dyn/cm^2) and the bulk modulus of silicon (3.7×10^{11} dyn/cm^2), respectively,[25] δ is the liner misfit, and $S(\beta, R)$ is the surface area of a precipitate. The liner misfit δ can be written as[22]

$$(1+\delta)^3 = \frac{\Omega_P/\Omega_M}{1+2\gamma_I}, \tag{16}$$

where Ω_M is the specific volume of a silicon atom (2×10^{-23} cm^3).[25] Figure 8 shows the values of β as a function of the precipitate radius R calculated under the condition that the excess free energy in Eq. (13) is minimized. The values of γ_I used here are obtained from the Arrhenius plots shown in Fig. 7 as follows:

$$\gamma_I = 3.6\times10^8 \exp(-2.32\text{eV}/kT). \tag{17}$$

The calculated results are in good agreement with the aspect ratio ranging from 0.007 to 0.03 as observed by Sueoka *et al.* after annealing at 700, 800, 900, and 1000 °C.[21,22,39] It is noted that polyhedral precipitates are observed after annealing at temperatures higher than 1000 °C.[25,40] As one can see in Fig. 7, the value of γ_I extrapolated to higher temperatures reaches the entire strain relaxation value[22] of 0.6 at about 1050 °C, which agrees with the formation temperature of polyhedral precipitates.

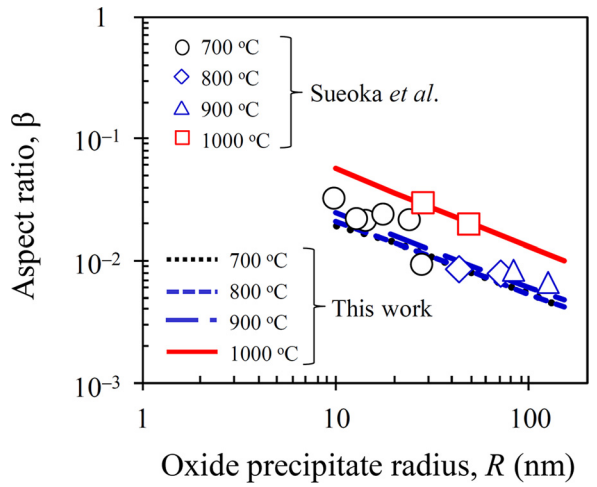

FIG. 8. Aspect ratio as a function of the radius of oxide precipitates obtained by TEM observations after annealing at 700 °C (circles), 800 °C (diamonds), 900 °C (triangles), and 1000 °C (squares).[21,22,39] The dotted, short-dashed, long-dashed, and solid lines show the corresponding aspect ratio calculated using the fraction of self-interstitial emission in Fig. 7.

IV. CONCLUSION

The enhancement of boron diffusion in $p/p+$ silicon epitaxial wafers with an oxide precipitate density of 10^8–10^{10} cm^{-3} has been investigated analyzing out-diffusion profiles obtained by SIMS after annealing at 850–1000 °C. It is found that the boron diffusion is enhanced with the increase of the oxide precipitate density. On the basis of the model for boron diffusion mediated by silicon self-interstitials, it is revealed that the enhanced diffusion is attributed to self-interstitials supersaturated as a result of the emission from oxide precipitates and the absorption by punched-out dislocations. The fraction of self-interstitial emission from oxide precipitates obtained analyzing the diffusion enhancement decreases with decreasing temperature, suggesting that the fraction is determined by $D_I C_I^{eq}/D_O C_O^{eq}$.[22] The morphology changes of oxide precipitates reported in the literature are well explained by the thermodynamic model considering its interfacial energy and strain energy depending on the fraction of self-interstitial emission obtained in this study.

[1]D. A. Antoniadis and I. Moskowitz, J. Appl. Phys. **53**, 6788 (1982).
[2]S. Matsumoto, Y. Ishikawa, and T. Niimi, J. Appl. Phys. **54**, 5049 (1983).
[3]D. Mathiot and J. C. Pfister, J. Appl. Phys. **55**, 3518 (1984).
[4]P. A. Packan and J. D. Plummer, J. Appl. Phys. **68**, 4327 (1990).
[5]T. T. Fang, W. T. C. Fang, P. B. Griffin, and J. D. Plummer, Appl. Phys. Lett. **68**, 791 (1996).
[6]H.-J. Gossmann, T. E. Haynes, P. A. Stolk, D. C. Jacobson, G. H. Gilmer, J. M. Poate, H. S. Luftman, T. K. Mogi, and M. O. Thompson, Appl. Phys. Lett. **71**, 3862 (1997).
[7]A. Ural, P. B. Griffin, and J. D. Plummer, J. Appl. Phys. **85**, 6440 (1999).
[8]H. Bracht, Phys. Rev. B **75**, 035210 (2007).
[9]H. Bracht, H. H. Silvestri, I. D. Sharp, and E. E. Haller, Phys. Rev. B **75**, 035211 (2007).
[10]S. T. Dunham, J. Appl. Phys. **71**, 685 (1992).
[11]S. Mizuo, T. Kusaka, A. Shintani, M. Nanba, and H. Higuchi, J. Appl. Phys. **54**, 3860 (1983).
[12]N. E. B. Cowern, G. F. A. van de Walle, D. J. Gravesteijn, and C. J. Vriezema, Phys. Rev. Lett. **67**, 212 (1991).
[13]J. Zhu, T. Diaz dela Rubia, L. H. Yang, C. Mailhiot, and G. H. Glimer, Phys. Rev. B **54**, 4741 (1996).
[14]J.-W. Jeong and A. Oshiyama, Phys. Rev. B **64**, 235204 (2001).
[15]H. Tsuya, Y. Kondo, and M. Kanamori, Jpn. J. Appl. Phys. **22**, L16 (1983).
[16]S. Matsumoto, I. Ishihara, H. Kaneko, H. Harada, and T. Abe, Appl. Phys. Lett. **46**, 957 (1985).
[17]D. A. P. Bulla, W. E. Castro, Jr., V. Stojanoff, F. A. Ponce, S. Hahn, and W. A. Tiller, J. Cryst. Growth **85**, 91 (1987).
[18]S. Hahn, F. A. Ponce, W. A. Tiller, V. Stojanoff, D. A. P. Bulla, and W. E. Castro, Jr., J. Appl. Phys. **64**, 4454 (1988).
[19]W. Wijaranakula, J. Appl. Phys. **72**, 4026 (1992).
[20]T. Ono, E. Asayama, H. Horie, M. Hourai, M. Sano, H. Tsuya, and K. Nakai, Jpn. J. Appl. Phys. **36**, L249 (1997).
[21]K. Sueoka, M. Akatsuka, M. Yonemura, T. Ono, E. Asayama, and H. Katahama, J. Electrochem. Soc. **147**, 756 (2000).
[22]K. Sueoka, N. Ikeda, T. Yamamoto, and S. Kobayashi, J. Appl. Phys. **74**, 5437 (1993).
[23]K. Sueoka, M. Akatsuka, M. Okui, and H. Katahama, J. Electrochem. Soc. **150**, G469 (2003).
[24]W. J. Taylor, U. Gösele, and T. Y. Tan, J. Appl. Phys. **72**, 2192 (1992).
[25]K. Sueoka, N. Ikeda, T. Yamamata, and S. Kobayashi, J. Electrochem. Soc. **141**, 3588 (1994).
[26]T. Y. Tan and W. K. Tice, Philos. Mag. **34**, 615 (1976).
[27]M. Tanaka, G. S. Liu, T. Kishida, K. Higashida, and I. M. Robertson, J. Mater. Res. **25**, 2292 (2010).
[28]M. W. Jenkins, J. Electrochem. Soc. **124**, 757 (1977).

[29]K. Torigoe, J. Fujise, T. Ono, and K. Nakamura, J. Appl. Phys. **116**, 193503 (2014).
[30]R. A. Craven, in *Semiconductor Silicon*, edited by H. R. Huff, R. J. Kriegler, and Y. Takeishi (The Electrochemical Society, Pennington, NJ, 1991), Vol. PV81-5, p. 254.
[31]G. Kissinger, D. Kota, J. Dabrowski, V. Akhmetov, A. Sattler, and W. von Ammon, ECS Trans. **16**(6), 97 (2008).
[32]K. Nakamura, T. Saishoji, and J. Toomioka, Solid State Phenom. **82-84**, 25 (2002).
[33]S. Senkader, P. R. Wilshaw, and R. J. Falster, J. Appl. Phys. **89**, 4803 (2001).
[34]J. D. Murphy, P. R. Wilshaw, B. C. Pygall, S. Senkader, and R. J. Falster, J. Appl. Phys. **100**, 103531 (2006).
[35]Z. Zeng, J. D. Murphy, R. J. Falster, X. Ma, D. Yang, and P. R. Wilshaw, J. Appl. Phys. **109**, 063532 (2011).
[36]J. C. Mikkelsen, Jr., Mater. Res. Soc. Symp. Proc. **59**, 19 (1985).
[37]W. A. Tiller, S. Hahn, and F. A. Ponce, J. Appl. Phys. **59**, 3255 (1986).
[38]F. R. N. Nabarro, Proc. R. Soc. A **175**, 519 (1940).
[39]K. Sueoka, M. Akatsuka, H. Katahama, and N. Adachi, J. Electrochem. Soc. **144**, 1111 (1997).
[40]H. Fujimori, J. Electrochem. Soc. **144**, 3180 (1997).